SGLT2 independent effects of the SGLT2 inhibitor empagliflozin

Focus on the heart

Chen, S.

Publication date
2024

Chapter 05

Empagliflozin mitigates cardiac hypertrophy through cardiac RSK/NHE-1 inhibition

Sha Chen, Kenneth Overberg, Zakiya Ghouse, Markus W Hollmann, Nina C Weber, Ruben Coronel, Coert J Zuurbier

Biomedicine & Pharmacotherapy 174:116477, 2024

Abstract

Background: Sodium glucose co-transporter 2 inhibitors (SGLT2i) reduce cardiac hypertrophy in type 2 diabetes (T2D), pulmonary arterial hypertension and left ventricular heart failure. The underlying mechanisms remain unknown. Cardiac serine/threonine kinases (STK) and sodium hydrogen exchanger 1(NHE1) activities are important regulators of cardiac hypertrophy and function. Whereas it is known that SGLT2i affect cardiac NHE1 directly, this is unknown for STK. Therefore, we first explored whether the SGLT2i empagliflozin (EMPA) has direct cardiac effects on STK in type II diabetic mice hearts. Subsequently, emerging STK target(s) from this analysis, together with NHE1 as known direct cardiac target of SGLT2i, were then further examined for their role in cardiac cell hypertrophy and its mitigation by EMPA in H9c2 cardiac cells.

Methods: Isolated hearts from db/db mice were perfused for 35 min with 1 µM EMPA, and STK phosphorylation sites were examined using unbiased multiplex analysis to detect the most affected STKs by EMPA. Subsequently, hypertrophy was induced in H9c2 cells with 50 µM phenylephrine (PE), and the role of the most affected STK (p90 ribosomal S6 kinase (RSK)) and NHE1 activity in hypertrophy and the protection by EMPA was evaluated.

Results: In db/db mice hearts, EMPA most markedly reduced STK phosphorylation sites regulated by RSKL1, a member of the RSK family, and by Aurora A and B kinases. GO and KEGG analysis suggested that EMPA inhibits hypertrophy, cell cycle, cell senescence and FOXO pathways, illustrating a general inhibition of growth pathways. The potential role of RSK in cardiac hypertrophy was further explored in H9c2 cells. EMPA prevented PE-induced hypertrophy as evaluated by BNP and cell surface area in H9c2 cells, mimicking in vivo effects. EMPA blocked PE-induced activation of NHE1. The specific NHE1 inhibitor Cariporide also prevented PE-induced hypertrophy without added effect of EMPA. EMPA significantly blocked PE-induced increase of RSK phosphorylation. The RSK inhibitor BIX02565 also suppressed PE-induced hypertrophy without added effect of EMPA. Cariporide mimicked EMPA's effects on PE-treated RSK phosphorylation. BIX02565 decreased PE-induced NHE1 activity, with no further decrease by EMPA.

Conclusions: RSK inhibition by EMPA treatment in isolated T2D mice hearts is a novel direct cardiac target of SGLT2i. Direct cardiac effects of EMPA exert their anti-hypertrophic effect through NHE-inhibition and subsequent RSK pathway inhibition.

Keywords: sodium glucose co-transporter 2 inhibitors (SGLT2i), sodium hydrogen exchanger 1 (NHE1), p90 ribosomal S6 Kinase (RSK), hypertrophy, Aurora, FoxO pathways

1.Introduction

Sodium glucose co-transporter 2 inhibitors (SGLT2i) are now used to treat heart failure (HF) patients independent of their diabetic status[1]. SGLT2i target the kidney, but the reported effects on glycosuria, hemodynamics and metabolism are unlikely to fully explain the cardiovascular benefits. Indeed, we recently demonstrated that the SGLT2i empagliflozin (EMPA) reduced infarct size equally in wild-type and SGLT2 knockout mice, suggesting that cardiovascular benefits of SGLT2i's against infarct development during ischemia-reperfusion of the heart are not through SGLT2[2 3]. One important cardiovascular beneficial effect of SGLT2i's is the reduction or attenuation of cardiac hypertrophy during the development of heart failure. SGLT2i decrease left ventricle (LV) mass in diabetic and non-diabetic HF patients and animals[4-7]. The mechanism of these beneficial cardiac effects are unknown.

Preclinical and clinical studies indicated that inhibition of the cardiac sodium hydrogen exchanger 1(NHE1) is effective in reducing or preventing cardiac hypertrophy and HF[8-12]. We and others earlier demonstrated direct inhibition of cardiac NHE1 activity by SGLT2i[13-15]. Thus, the decrease of cardiac hypertrophy by SGLT2is may, at least partly, be mediated through NHE1 inhibition. However, experimental data to support this hypothesis are currently missing.

Serine/threonine kinases (STK) are known regulators of the NHE1 and involved in cardiac hypertrophy[16]. We hypothesize that STKs are modulated by SGLT2i. Therefore, we first apply an differential integrated kinomics approach between control and EMPA-perfused diabetic mice hearts for the evaluation of global profile changes of STK phosphorylation sites, and subsequent bioinformatics analysis to identify cardiac STK kinases that are affected by SGLT2i and may play a role in cardiac pathological hypertrophy. Next, we test the effect of NHE1 and the most prominent emergent STK on its contribution to the prevention of cardiac hypertrophy through the application of EMPA in a cardiac cellular model.

.

2. Methods

2.1 Isolated db/db mice hearts

For cardiac kinome analysis we examined freeze-dried cardiac tissue from Langendorff-perfused hearts of db/db male mice from our previously reported study of EMPA effects on cardiac metabolism[17]. In short, these hearts were isolated and perfused (37 ^{o}C Celsius, pH 7.35-7.45), at an initial perfusion pressure of 80 mm Hg with a constant flow with Krebs-Henseleit (KH) buffer [(in mmol/l), 118 NaCl, 4.7 KCl, 1.2 $MgSO_4$, 1.2 KH_2PO_4, 25 $NaHCO_3$, 0.5 EDTA, 2.50 $CaCl_2$, 5.5 D-glucose, 0.5 L-glutamine, 1 lactate, 0.1 pyruvate, 1% (g/l) albumin-0.4 mM palmitic acid sodium salt, 0.05 L-carnitine, and 30 mU/l insulin]. Two groups were studied (n=8 each group): one group perfused for 35 min with DMSO vehicle (0.02% final concentration), whereas the other group was perfused for 35 min with DMSO+EMPA (1µM final concentration). Afterwards, the hearts were immediately frozen in liquid nitrogen, freeze-dried overnight, and stored at -80 °C for further analysis. Animal handling was in accordance with the Institutional Animal Care and Use Committee of Amsterdam UMC, location AMC, and was performed in accordance with guidelines from Directive 2010/63/EU of the European Parliament on the protection of animals used for scientific purposes.

2.2 PamGene serine/threonine kinases

The kinase activity assessment of db/db mice hearts was conducted using PamChip STK Array Chips and a PamStation 12 system, following the manufacturer's instructions. Briefly, hearts from 16 db/db mice, divided into EMPA and DMSO groups (n=8 each), were lysed in M-PER Mammalian Extraction Buffer. For the STK Array, 2 µg of cleared cellular lysate was mixed with 4 µl of 10 × PK buffer, 0.4 µl of 100 × bovine serum albumin (BSA), and 1 µl of 4 mM ATP, which was then adjusted to 40 µl with distilled H_2O. Each array was blocked with 0.2% BSA and washed using PK solution. Subsequently, a kinase reaction was conducted at 30 °C. The reaction mix was pulsed through the PamChip for 60 cycles. Next, the Detection Mix, consisting of 3 µl of 10 × Antibody buffer, 0.34 µl of STK antibody mix, and 0.4 µl of FITC-labeled STK antibody, adjusted to 30 µl with distilled H_2O, was applied to the chip. The reaction mix was then pulsed through the PamChip for an additional 30 cycles.

Spot intensities were normalized using BioNavigator (PamGene) software by subtracting the median background signal from the median spot intensity. Additionally, a constant background of 40 was subtracted from each raw median signal, based on a preliminary experiment using an empty blanco array.

To ensure comparability and to remove typical mean-variance dependency, the data were further normalized using the 'Variance stabilizing normalization (VSN)' method. All analyses were performed using R software. By comparing the samples from the EMPA and DMSO groups, differentially phosphorylated peptides were

identified using linear models. The log2 fold change (log2 FC) was then assessed to determine whether the phosphorylation of peptides was upregulated or downregulated[18,19].

2.3 Functional and pathway enrichment analysis

The gene names of predicted kinases with down-regulated phosphorylation were all used for gene ontology (GO) and Kyoto Encyclopedia of Genes and Genomes (KEGG) analysis. The cluster Profiler package of the R language was used to classify and visualize biological processes (BP) via GO analysis[20]. This package was also used to perform KEGG pathway enrichment analysis. In both the GO and KEGG analyses, an adjusted P-value (p.adjust) <0.05 was considered as the cut-off point. We only showed the top 20 BPs and pathways.

2.4 Cell culture

H9c2 rat cardiomyoblast cells were obtained from ATCC (American Type Culture Collection, Manassas, Virginia, USA) and cultured in high glucose (4,500 mg/l) Dulbecco's modified Eagle's medium (DMEM) supplemented with 10% Fetal Calf Serum (FCS) and 100 U/ml of Penicillin/Streptomycin. Cells were recovered by centrifugation (5 min, 1000 rpm), re-suspended in plating medium. Cells were grown in an atmosphere of 95% O_2, 5% CO_2 in a humidified incubator. Stock cultures were passaged at 2- to 3-day intervals. To induce hypertrophy, the cells were starved by reducing FCS from 10% to 1% for 24 h in DMEM and subsequently incubated with 50 µM PE (Sigma, #P1240000) up to 48 h. Cells were then seeded at a density of 1.4×10^3 cells per well in 6-well plates for cell surface area measurement. For immunoblot analysis, NHE1 activity and RNA extraction, cells were seeded at a density of 5×10^4 cells per well in 6-well plates. H9c2 cardiomyoblasts were treated for 48 h with different treatments.

The following cell treatments were examined and compared: The vehicle (V) group was subjected to DMSO (0.02%). The PE (P+V) group was given 50 µM PE and 0.02% DMSO. The PE+EMPA (P+E) group was given 50 µM PE and 1 µM EMPA (MedChem Express, # HY-15409). EMPA (E) group was exposed to 1 µM EMPA. PE+ BIX02565 (P+B) group was treated with 50 µM PE and 1 µM BIX02565[21] (MedChem Express, # HY-16104, RSK inhibitor). PE+EMPA+ BIX02565 (P+E+B) group was subjected to 50 µM PE, 1 µM EMPA and 1 µM BIX02565. PE+Cariporide (P+C) group was treated with 50 µM PE and 10 µM Cariporide (NHE1 inhibitor). PE+EMPA+Cariporide (P+E+C) group was treated with 50 µM PE, 1 µM EMPA and 10 µM Cariporide. EMPA, BIX02565 and Cariporide are all dissolved into 0.02% DMSO.

2.5 Quantitative real time PCR (RT-PCR)

Total RNA from H9c2 cell line was extracted using TriPure™ isolation reagent (Sigma, #11667157001) and cDNA was synthetized by Transcriptor First Strand cDNA Synthesis Kit (Roche, # 4897030001), following the manufacturer instruction. After the reverse transcription reaction, RT-PCR was performed with the SYBR Green real time PCR master mix kit (Roche, # 4707516001). The reaction was visualized by SYBR Green Analysis on LightCycler® 480 System (Roche). Primers for gene analysis were as follows: ANF: For 5'CCTCTTCCTGGCCTTTTGG3'; Rev 5'CCAGGTGGTCTAGCAGGTTCTT3'; BNP: For 5'AGGAGAGACTTCGAAATTCCAAGA3'; Rev 5'CTAAAACAACCTCAGCCCGTCA. GAPDH: For 5' TCGGTGTGAACGGATTTGGC3'; Rev 5'TCCCATTCTCGGCCTTGACT3'. Thermal cycling was initiated with an initial denaturation at 95 °C for 10 min. After this initial step, 40 cycles of PCR were performed. Each PCR cycle consisted of heating at 95 °C for 10 sec. for melting, 60 °C for 10 sec for annealing and 72 °C for 15 sec for the extension. 37 °C for 30 sec for cooling. The ratio of fold change was calculated using the Pfaffl method[22].

2.6 Determination of cell surface area

For analysis of morphometric hypertrophy, the size of the cells was measured utilizing IncuCyte® Live Cell Imager system (Sartorius, Essen Biosciences). After 48 h of treatment with various compounds (see table 1), the cell culture plates were placed into the Incucyte Live cell imager and images were taken automatically and blindly. Blinded cell surface area analysis was performed using Image J software. A minimum of 30 cells per group was examined and data is normalized to V group in order to facilitate comparison of relative cell surface area across treatments.

2.7 Western blotting

A Lowry assay was used to determine protein concentration. Western blotting was conducted as described previously[23]. In brief, equal amount of protein per sample was electrophoresed on a 4-12% precast polyacrylamide gel (Bio-Rad, #345-0125) and transferred to polyvinylidene fluoride (PVDF) membrane. After incubation with blocking buffer (Odyssey, #927-70001) for 1 h, the membrane was probed with primary antibody for GAPDH (Abcam, #ab9484, 1:5000); NHE1(Sigma, # MAB3140, 1:1000); p90RSK (Thr359/Ser363) (Cell Signaling Technology, #9344S, 1:100) and RSK1/2/3 (Cell Signaling Technology, #9355S, 1:100) overnight at 4 °C. Membranes were washed with PBS-Tween 20 and incubated with the complementary secondary fluorescence antibody (LI-COR Biosciences, goat anti-rabbit #926-68071/926-32211 or goat anti-mouse #926-32210, 1:5000) for 1 h at room temperature. Membranes were washed again and scanned with Odyssey scanner (LI-COR). Membranes were subjected to Coomassie blue (Bio-Rad, # 1610786) staining to confirm equal loading of protein.

2.8 NHE1 activity measurement

5×10^4 cells per well were cultured on a gelatin-coated coverslip in a 6-well plate to determine activity of NHE1 following the various treatments by PE, EMPA, Cariporide (specific NHE1 inhibitor) and BIX02565 (RSK inhibitor). After the 48 h treatment, the coverslips containing the cells were treated with the pH fluorescent probe of 10 µM SNARF-AM (Thermo Fisher Scientific, #C1270) for 30 min at 37 °C. Then cells were placed inside a perfusion chamber (height 0.4 mm, diameter 10 mm, volume 30 µl) on an inverted fluorescence microscope (Nikon Diaphot, Tokyo, Japan) at 37 °C. The NHE1 activity was measured by recording SNARF-fluorescence (580/640 nm emission; 515 nm excitation) following a NH_4^+ pulse[24]. Briefly. after a 30-sec stabilization period, the medium was rapidly (< 1 sec) exchanged with the same solution now containing 20 mM NH_4Cl for 10 min, inducing intracellular alkalosis. Subsequently, the NH_4Cl-containing medium was swiftly replaced (<1 sec) with a normal solution, leading to near-instantaneous intracellular acidosis. The subsequent recovery from acidosis was monitored for the following 5 min. NHE1 activity was reflected by the slope of a linear fit over first 50 s of intracellular $[H^+]$ recovery. The effects with different treatments were tested on recovery of acidosis and these compounds were continuously present during the NH_4Cl pulse and the washout period of NH_4Cl.

2.9 Statistics

Statistical analysis was performed using GraphPad Prism v9. Results are presented as mean ± SD. Data normality was examined using the Shapiro-Wilk test (with α=0.05). For normally distributed data, a unpaired t-test was used for two-group analysis and one-way ANOVA with Holm-Šidák multiple comparisons was used for multiple-group analysis. For non-normally distributed data, the Kruskal-Wallis test with Dunn's multiple comparisons test was used for multiple-group analysis. The significance level for all tests was set to α=5%. *P value<0.05; **P value<0.01; ***P value<0.001 and ****P value<0.0001; ns: not significant

3. Results

3.1 EMPA acutely decreases STK activities in the diabetic heart

Acute EMPA treatment led to a general inhibition of STK activity, resulting in decreased phosphorylation of 13 peptides **(Fig. 1A).** Based on the detailed pattern of differential peptide phosphorylation between the two groups, the specific profile for the distinct substrates was used to predict the reduced activity of the top 30 ranked kinases in (**Fig. 1B)**. In db/db hearts, EMPA significantly inhibited several RSK kinases, with largest effects observed for RSKL1, a member of 90 kD ribosomal S6 kinase (RSK) family **(Fig. 1B**). The second largest EMPA effects were observed for Aurora kinases. These kinases are known to play a role in cell division by controlling centrosome biology and spindle assembly. The 20 most relevant biological processes from GO and pathways from KEGG database, sorted by false discovery rate, are presented (**Fig. 1C-D)**. From the GO analysis, we observed that STK with EMPA-reduced activity have been associated with cardiac hypertrophy reduction, next to the expected effects on serine-threonine phosphorylation and processes related to the cell cycle. KEGG analysis showed that these predicted kinases were likely to be involved in FoxO pathway, cell senescence and MAPK signaling.

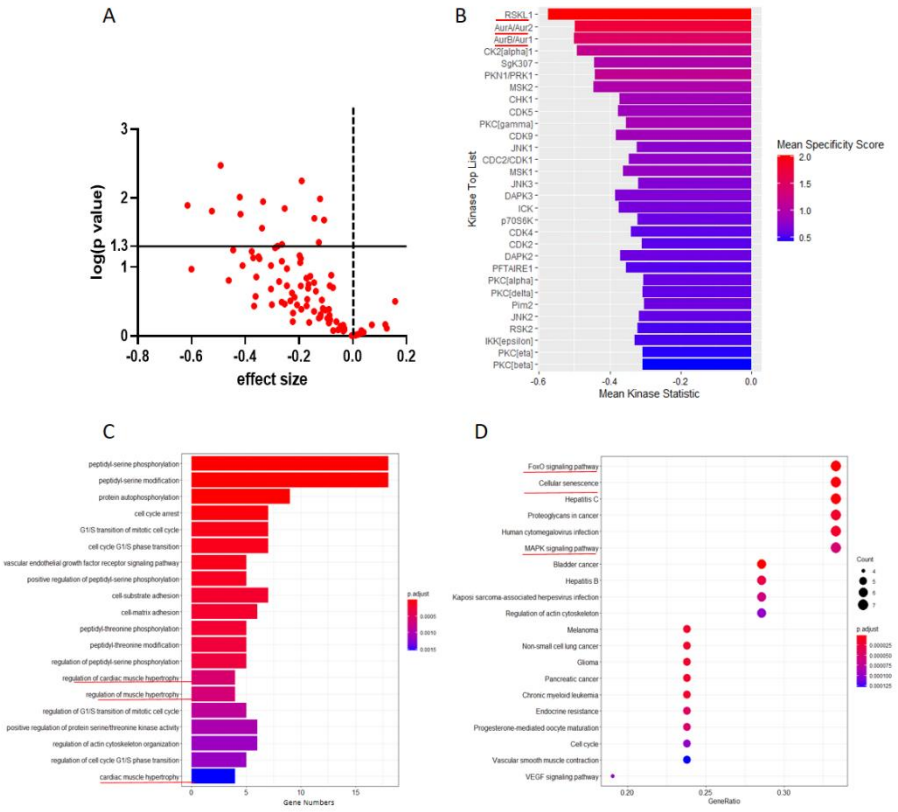

Figure 1. EMPA reduces STK activity in the isolated db/db mice hearts. Volcano plot showing decreased STK phosphorylation sites by EMPA treatment (**A**). Top 30 STK with predicted down-regulated activity derived from the altered STK phosphorylation sites (**B**). The associated biological processes and pathways that are most influenced by the predicted changed STK activity due to EMPA treatment as a result of GO and KEGG analysis (**C-D**). Gene numbers reflect number of genes within one biological process that are down-regulated by the predicted alterations in STK. Gene ratio was the ratio of gene numbers affected by EMPA relative to the total number of genes of that pathway. The size of circle represents gene count. Different colors of the circles represent different adjusted p values. Vehicle treated db/db mice hearts (n=8) versus EMPA treated db/db hearts (n=8).

3.2 EMPA prevents cellular hypertrophy induced by PE in the absence of SGLT2 in H9c2-cells

RT-PCR analysis demonstrated that 50 µM PE increased BNP mRNA expression, without change of ANP mRNA expression. EMPA was able to prevent the PE-induced elevation of BNP mRNA expression (**Fig. 2A and Supple Fig. 1A**). Correspondingly, the cell surface area was increased by PE, and EMPA was able to prevent PE-induced increase of cell surface area (**Fig. 2B**). EMPA had no effect on BNP mRNA expression and cell surface area in non-treated H9c2 cells (**Suppl. Fig. 1 B-C**). No SGLT2 protein expression in H9c2 cells was detected. Wild type kidney cells from C57BL/6N mice[2] served as a positive control (SGLT2 antibody) and SGLT2 knock-out as a negative control (**Fig. 2C)**.

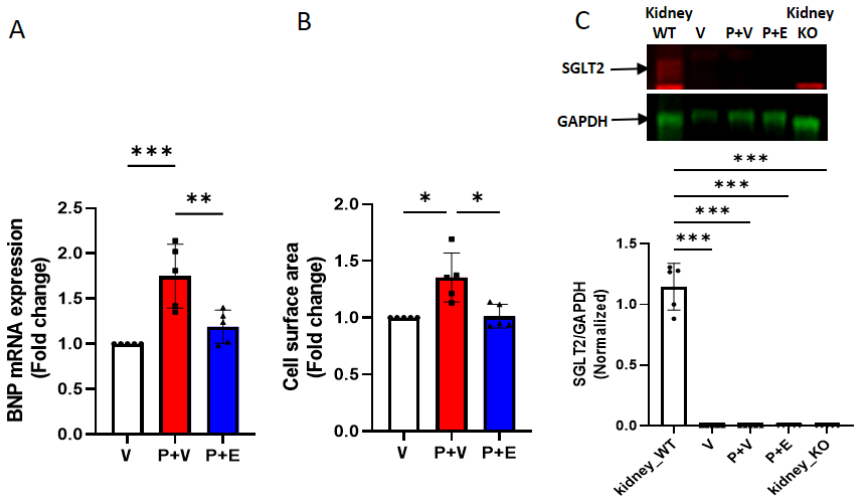

Figure 2. EMPA inhibits PE-induced cellular hypertrophy in H9c 2 cells that are devoid of SGLT2. A: Phenylepinephrine (P) increased BNP mRNA expression, whereas EMPA (E) treatment attenuated BNP increases. One way ANOVA with Holm-Šídák's multiple comparisons test. **B**: Phenylepinephrine (P) increased cell surface area, whereas EMPA (E) treatment prevented increase in cell surface area by P; for each condition at least 30 cells were counted in each individual experiment. Kruskal-Wallis test with Dunn's multiple comparisons test. **C**: Representative immunoblots and analysis of SGLT2 showing SGLT2 to be present in wild type kidney, but not in H9c2 cells treated with vehicle (V), phenylephrine (P) or Empa (E). SGLT2 KO kidney is used as a negative control for the AB SGLT2. Kruskal-Wallis test with Dunn''s multiple comparisons test. Data are presented as mean ± SD. *p < 0.05, ** p < 0.01, *** p < 0.001. ns: not significant. All experiments employed 5 independent experiments.

3.3 EMPA reduces PE-induced hypertrophy through NHE1 inhibition

In order to determine whether NHE1 was involved in PE-induced hypertrophy and EMPA's protection in our model, we examined NHE1 protein expression and activity. NHE1 protein expression was not altered with PE or PE plus

EMPA treatment (**Fig. 3A**). However, NHE1 activity was increased by PE treatment, whereas EMPA or 10 μM cariporide almost completely prevented PE-induced activation of NHE1 (**Fig. 3B-D**). Additionally, inhibition of NHE1 by cariporide prevented the PE-induced increases of BNP and cell surface area. Furthermore, compared with EMPA treatment alone, the combination of cariporide and EMPA did not further reduce these two hypertrophic parameters of H9c2 cells exposed to PE, suggesting that the anti-hypertrophic action of EMPA is mediated through NHE1 inhibition (**Fig. 3E-F**).

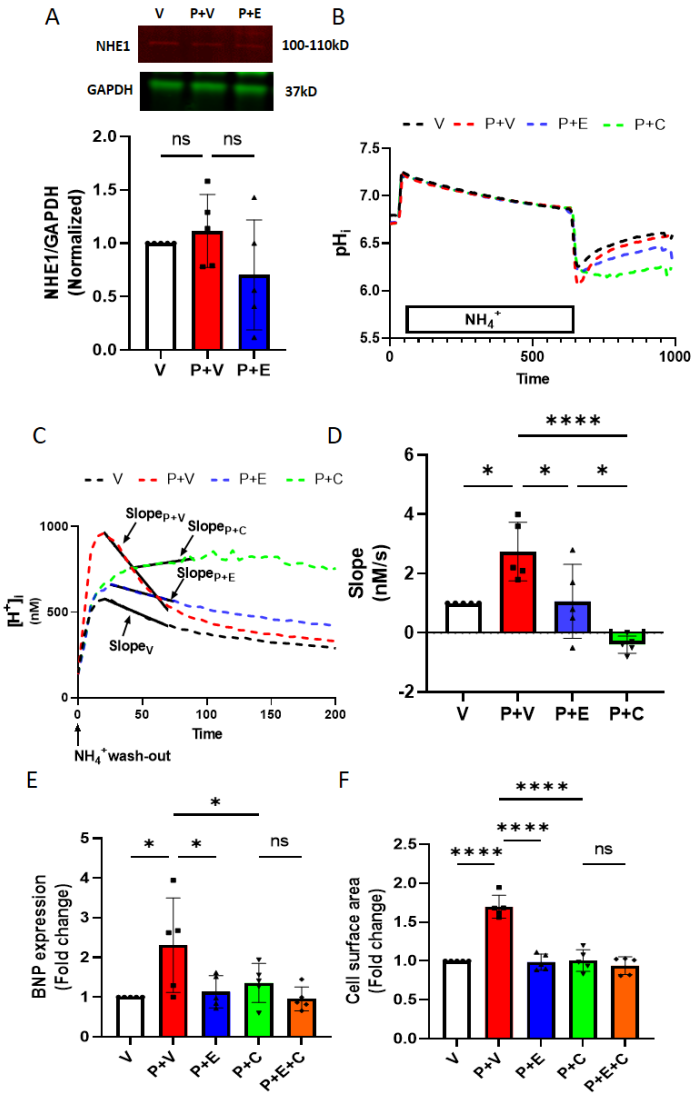

Figure 3. EMPA reduces PE-induced hypertrophy through NHE1 Inhibition. **A**: Representative immunoblots and analysis of NHE1 protein in H9c2 cells under different conditions. One way ANOVA with Holm-Šídák's multiple comparisons test. **B**: Intracellular pH during an $NH4^+$-pulse in cells treated with vehicle, phenylepinephrine (P), P plus EMPA (E) or P plus Cariporide (C). **C**: Intracellular $[H^+]$ during the first 200 sec after NH_4^+ wash-out, showing the fitted slope of $[H^+]$ recovery as index of NHE1 activity for vehicle, P, P+ E or P+C. **D**: NHE1 activity as reflected by the fitted slope of $[H^+]$ recovery). One way ANOVA with Holm-Šídák's multiple comparisons test. **E**: BNP mRNA expression was measured by RT-PCR after 48 h treatment under each condition. One way ANOVA with Holm-Šídák's multiple comparisons test. **F**: Cell surface area was measured at 48 h, and at least 30 cells were counted from each condition in each individual experiment. One way ANOVA with Holm-Šídák's multiple comparisons test. Slope ($\Delta[H^+]/\Delta s$) is the linear fit over first 50 s of intracellular $[H^+]$ recovery. Data are presented as mean ± SD. * $p < 0.05$, **** $p < 0.0001$. ns: not significant. All data based on 5 individual experiments.

3.4 EMPA reduces PE-induced hypertrophy through RSK inhibition.

PE-induced hypertrophy was indeed associated with increases in p-RSK, and this effect was totally abrogated in the presence of EMPA (**Fig. 4A**). In addition, the RSK inhibitor BIX02565 (1 μM), (labeled B in figures 4 and 5) was able to completely reverse the PE-induced increases in BNP and cell surface area. Thus, RSK inhibition mitigated PE-induced hypertrophy. Furthermore, compared with BIX02565, the combination of BIX02565 and EMPA did not further decrease BNP and cell surface area, indirectly suggesting that RSK inhibition regulate anti-hypertrophic pathways similar as EMPA (**Fig. 4B-C**).

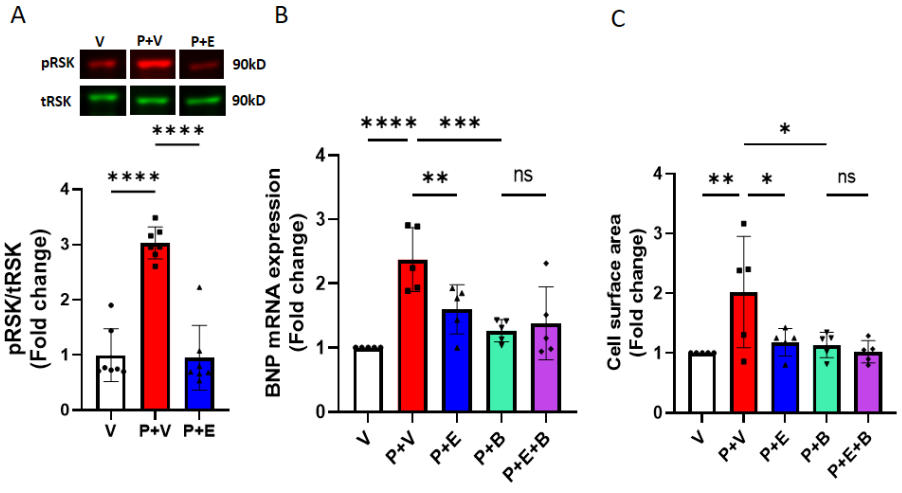

Figure 4. RSK activation/phosphorylation is involved in PE-induced hypertrophy and EMPA's protection against hypertrophy. **A:** Representative immunoblots and analysis of phosphorylated RSK (pRSK) and total RSK (tRSK), showing activated RSK with phenylepinephrine (P) treatment, with activation mitigated by Empa (E) treatment. Kruskal-Wallis test with Dunn''s multiple comparisons test (n=7 independent experiments). **B-C**: P-induced cardiac cell hypertrophy, indicated by BNP (**B**) and cell surface area H9c2 cells (**C**), with hypertrophy equally reduced by Empa (E) or RSK inhibitor BIX02565 (B), without additive effects of E and B. One way ANOVA with Holm-Šídák's multiple comparisons test. (n=5 individual experiments). Data are presented as mean ± SD. * $p < 0.05$, ** $p < 0.01$, *** $p < 0.001$, **** $p < 0.0001$. ns: not significant.

3.5 NHE1 inhibition decreases RSK activity, and RSK inhibition decreases NHE1 activity

We then examined whether NHE1 inhibition can decrease PE-induced RSK activation**.** Indeed, cariporide prevented the PE-induced p-RSK increase, which could not be further decreased by EMPA (**Fig. 5A**). Vice versa, NHE1 activity measurement showed that RSK inhibition with BIX02565 reduced PE-induced activation of NHE1, and adding EMPA to BIX02565 did not further reduce NHE1 activity(**Fig. 5B-D**).

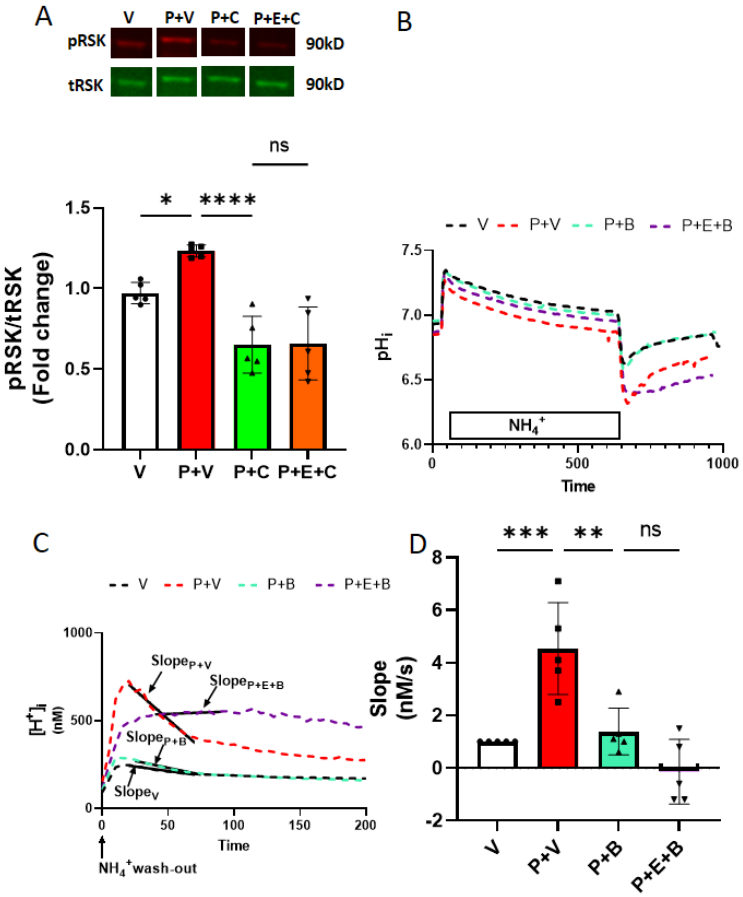

Figure 5. NHE1 inhibition decreases RSK activation, and RSK inhibition decreases NHE1 activatio. A: Representative immunoblots and analysis of RSK, showing NHE1 inhibitor cariporide (C) reduced phenylepineprhine (P)-induced RSK activation relative to vehicle (V)-treated groups, negating any additive reducing effects of EMPA (E). One way ANOVA with Holm-Šídák's multiple comparisons test. **B**: Average curve changes of intracellular pH in cells treated with vehicle, P, P+BIX02565 (B) or P+E+B. **C**: Intracellular [H^+] during the first 200 sec after NH_4^+ wash-out, showing the fitted slope of [H^+] recovery as index of NHE1 activity for V, P, vehicle, P, P+B or P+E+B. **D**: NHE1 activity as reflected by the fitted slope of [H^+] recovery). One way ANOVA with Holm-Šídák's multiple comparisons test. Slope ($\Delta[H^+]/\Delta s$) is the linear fit over first 50 s of intracellular [H^+] recovery. Data are presented as mean ± SD (n=5 individual experiments). * $p < 0.05$, ** $p < 0.01$, *** $p < 0.001$, **** $p < 0.000$. ns: not significant.

4. Discussion

The major findings of the present study can be summarized as follows: (1) the SGLT2 inhibitor EMPA negatively regulates various STK in the isolated diabetic heart, with largest reductions in RSK and Aurora A and B kinase activities, (2) EMPA alleviates PE-induced hypertrophy in a cardiac cellular model of hypertrophy, demonstrating direct cardiac anti-hypertrophic effects of SGLT2i's, and (3) the anti-hypertrophic cardiac effects of EMPA are mediated through bidirectional RSK-NHE1 inhibition.

4.1 Cardiac specific prevention of hypertrophy by EMPA

We employed an established cardiac cell model of PE-induced hypertrophy[25]. Our results clearly show that EMPA is able to prevent hypertrophy in this cardiac cell model. Similar direct cardiac cell effects were observed by Abdulrahman et al., showing that EMPA reduced angiotensin II-induced hypertrophy in H9c2 cardiomyoblasts[26]. SGLT2 protein expression was absent in our model. This is in contrast to reports by other groups reporting that EMPA's cardio-protective effect is mediated through reductions of cardiac SGLT2 levels[27,28]. Some SGLT2 antibodies not only bind to epitopes within SGLT2, but also within SGLT1, a protein that is present in heart[29]. The specificity of the SGLT2 antibody used in the present study had been verified by us in SGLT2 KO mice[2]. Additionally, our observation that the cardioprotective effects of EMPA against cardiac ischemia/reperfusion (I/R) injury are equally present in wild-type and SGLT2 knockout animals supports the concept that protective effects by SGLT2i are not mediated through SGLT2, but represent on off-target cardiac effect[2]. Hence, our data support the hypothesis that the improvement of hypertrophy by EMPA is mediated through a direct cardiac mechanism that is SGLT2 independent.

4.2 EMPA and the cardiac serine-threonine kinase kinome

Unbiased differential analysis of kinome STK activities revealed that direct cardiac effects of EMPA result in a global inhibition of serine-threonine kinase (STK) activities in type II diabetic heart. The top down-regulated STKs by EMPA were RSKL1, a member of the Ribosomal s6 kinase (RSK) family, and Aurora A and Aurora B kinases. These kinases are mostly involved in cell division and mitosis. Although the functional role of Aurora A and Aurora B in the post-mitotic heart is unclear, high activity of these kinases do contribute to the progression of cancers[30,31], suggesting therapeutic options for SGLT2i in cancer treatment[32,33].

The family of RSK are pleiotropic effectors for extracellular signal-regulated kinase signaling pathways. RSK3 transduces various pathological stimuli important for pathological remodeling of the heart and is considered as a therapeutic target for the prevention of HF[34]. Besides, cardiac-specific expression of a dominant negative RSK

mutant in transgenic mice is associated with improved myocardial resistance to I/R injury[35]. Furthermore, GO analysis of the observed altered phosphorylation sites with EMPA strongly suggests changes in kinases that are involved in cardiac hypertrophy . This is in agreement with reports showing reduction of cardiac hypertrophy by SGLT2i's[4-7]. Our KEGG analysis indicates that cardiac FoxO pathways are influenced by EMPA. FoxO pathways are important regulators of cardiac hypertrophy[36] and studies have already demonstrated SGLT2i-effects on FoxO in diabetic and hypertrophic hearts [36,37]. Thus, EMPA-mediated RSK alterations are involved in prevention of hypertrophy.

4.3 Anti-hypertrophic effects of EMPA are mediated through NHE1/RSK inhibition

NHE1, a multifunctional protein and a major cellular pH regulator, is instrumental in inducing cardiac hypertrophy through increased NHE1 activity following various pathological stimuli such as pressure overload, volume overload, excessive adrenergic activation and metabolic overloading [8-12,38,39]. Previous work from our group has unraveled that SGLT2i can directly bind to NHE1 and reduce its activity in rabbit and mouse cardiomyocytes[13,14]. Indeed, several groups have now demonstrated direct binding of SGLT2i to NHE1[40-43]. Other studies have shown that EMPA inhibits NHE1 activity also in fibroblast[44] and endothelial cells[24]. Moreover, EMPA ameliorates angiotensin II-induced hypertrophy in H9c2 cells via inhibition of NHE1 expression[26]. In contrast, some studies have failed to demonstrate interactions between SGLT2i and NHE1 activity[45-47]. This may, at least partly, be explained by cell isolation procedures employed[48].

Whether SGLT2i reduces cardiac hypertrophy through reduced NHE1 activity is unknown. In a recent study, Abdulrahman et al. demonstrated that EMPA reduced angiotensin II-induced hypertrophy and that this was also associated with reduced NHE1 protein expression.[26] However, a causal role for EMPA-mediated inhibition of NHE1 activity in reducing hypertrophy was not explored. The present study demonstrates that inhibition of NHE1 activity by EMPA may be causal to EMPA-mediated hypertrophy reducing effects: While cardiac NHE1 activity was increased with PE-induced hypertrophy, EMPA reduced this activity. Reduction of cardiac NHE1 activity by a specific inhibitor of NHE1, Cariporide, also reduced hypertrophy. In contrast to Abdulrahman study, no significant changes in NHE1 expression were observed.

The STK kinome analysis in the diabetic mice hearts revealed that RSK signaling is a major pathway influenced by EMPA. Subsequently, in our cellular model of hypertrophy we confirmed that direct cardiac effects of EMPA reduced phosphorylation of RSK. This is the first time that RSK is identified as a target for EMPA. Previous work demonstrated that RSK is an important regulator of NHE1 activation[49]. Inhibiting RSK phosphorylation prevented PE-induced activation of NHE1

in ventricular myocytes, suggestive that RSK is upstream of NHE1 activation[50]. In addition, Shi et al. have shown that I/R-activated RSK phosphorylates NHE1 at serine 703 (S703), which maintains NHE1 in a highly activated state[49]. Maekawa et al. have found that inhibition of RSK in cardiomyocytes prevents I/R-induced NHE1 activation[35]. However, other studies observed RSK to be downstream of NHE1. Jaballah et al. demonstrated that RSK becomes phosphorylated upon infection of H9c2 cells with an adenovirus containing the active form of NHE1[51]. Abdulrahman et al. have found that NHE1 transgenic overexpressed mice also shows upregulation of phosphorylation of RSK[52]. In the present study we demonstrate that the NHE1 inhibitor cariporide reduced RSK phosphorylation, confirming that RSK is downstream of NHE1. However, at the same time, we observed that the RSK inhibitor BIX02565 also resulted in decreased NHE1 activity, suggesting that RSK is upstream of NHE1. Thus, our results suggest a bidirectional interaction between NHE1 and RSK, as described for other regulatory systems[53].

The present study demonstrated that EMPA treatment decreases NHE1 activity as well as RSK phosphorylation. Most likely these effects are initially mediated through binding of EMPA to the NHE1 [13,15,40,42,54,55]. However, it was recently also reported that EMPA transfers to the intracellular compartment, increasing cytosolic and mitochondrially-produced ATP synthesis[54]. If this would indeed be the case, it would be possible that intracellular EMPA may then first impact on RSK signaling before NHE1 inhibition takes place.

4.4 Limitations of this study

For the analysis of EMPA-effects on STK in diabetic hearts only short term EMPA treatment (35 min) was examined. It cannot be excluded that long term treatment are more relevant to the human conditions, and will result in different effect. However, treatment of heart failure mice with EMPA for more than one week still reduced NHE1 activity of isolated cardiomyocytes, at least suggesting that NHE1 inhibition by EMPA is maintained over days (unpublished data from own research group).

Additionally, we have employed the rat cardiomyoblast cell culture H9c2 as a model for adult cardiomyocytes. Knowing that these H9c2 cells have low resemblance to mature adult cardiac tissue limits their translational value towards the human condition of cardiac hypertrophy that also usually is present only at the older age. However, H9c2 cells are more similar to primary cardiomyocytes than other cardiac cell lines, showing improved energy status and sensitivity to pathological events[56,57]. In addition, EMPA reduced RSK activity similarly in adult intact beating mouse hearts as in H9c2 cells, demonstrating that at least for these cellular pathways H9c2 cells mimic the adult mouse heart.

4.5 Conclusions

Acute EMPA treatment of type 2 diabetic mice hearts has a general inhibitory effect on serine-threonine kinases, with largest effects encountered for RSK and Aurora kinases. These result suggest that cardiac hypertrophy, cell cycle and FoxO pathways are influenced by direct cardiac effects of SGLT2i. Subsequently, we confirmed that EMPA protects against phenylephrine-induced hypertrophy through bidirectional NHE1/RSK inhibition. Our observations provide novel insights into the underlying cellular mechanisms of the cardio-protection by EMPA in the setting of HF.

4.6 Funding

The research was partly funded by the European Foundation for the Study of Diabetes (EFSD, 2018). S.C. is supported by a China Scholarship Council (CSC) fellowship program (201907000127).

References

1. Zannad F, Ferreira JP, Pocock SJ, et al. SGLT2 inhibitors in patients with heart failure with reduced ejection fraction: a meta-analysis of the EMPEROR-Reduced and DAPA-HF trials. Lancet 2020;396(10254):819-829. DOI: 10.1016/s0140-6736(20)31824-9.
2. Chen S, Wang Q, Christodoulou A, et al. Sodium Glucose Cotransporter-2 Inhibitor Empagliflozin Reduces Infarct Size Independently of Sodium Glucose Cotransporter-2. Circulation 2023;147(3):276-279. DOI: 10.1161/circulationaha.122.061688.
3. Chen S, Coronel R, Hollmann MW, Weber NC, Zuurbier CJ. Direct cardiac effects of SGLT2 inhibitors. Cardiovasc Diabetol 2022;21(1):45. DOI: 10.1186/s12933-022-01480-1.
4. Verma S, Mazer CD, Yan AT, et al. Effect of Empagliflozin on Left Ventricular Mass in Patients With Type 2 Diabetes Mellitus and Coronary Artery Disease: The EMPA-HEART CardioLink-6 Randomized Clinical Trial. Circulation 2019;140(21):1693-1702. DOI: 10.1161/circulationaha.119.042375.
5. Yurista SR, Silljé HHW, Oberdorf-Maass SU, et al. Sodium-glucose co-transporter 2 inhibition with empagliflozin improves cardiac function in non-diabetic rats with left ventricular dysfunction after myocardial infarction. Eur J Heart Fail 2019;21(7):862-873. DOI: 10.1002/ejhf.1473.
6. Santos-Gallego CG, Requena-Ibanez JA, San Antonio R, et al. Empagliflozin Ameliorates Adverse Left Ventricular Remodeling in Nondiabetic Heart Failure by Enhancing Myocardial Energetics. J Am Coll Cardiol 2019;73(15):1931-1944. DOI: 10.1016/j.jacc.2019.01.056.
7. Santos-Gallego CG, Vargas-Delgado AP, Requena-Ibanez JA, et al. Randomized Trial of Empagliflozin in Nondiabetic Patients With Heart Failure and Reduced Ejection Fraction. J Am Coll Cardiol 2021;77(3):243-255. DOI: 10.1016/j.jacc.2020.11.008.
8. Baartscheer A, Hardziyenka M, Schumacher CA, et al. Chronic inhibition of the Na+/H+ - exchanger causes regression of hypertrophy, heart failure, and ionic and electrophysiological remodelling. Br J Pharmacol 2008;154(6):1266-75. DOI: 10.1038/bjp.2008.189.
9. Avkiran M, Cook AR, Cuello F. Targeting Na+/H+ exchanger regulation for cardiac protection: a RSKy approach? Curr Opin Pharmacol 2008;8(2):133-40. DOI: 10.1016/j.coph.2007.12.007.
10. Karmazyn M, Kilić A, Javadov S. The role of NHE-1 in myocardial hypertrophy and remodelling. J Mol Cell Cardiol 2008;44(4):647-53. DOI: 10.1016/j.yjmcc.2008.01.005.
11. Baartscheer A, Schumacher CA, van Borren MM, Belterman CN, Coronel R, Opthof T, Fiolet JW. Chronic inhibition of Na+/H+-exchanger attenuates cardiac hypertrophy and prevents cellular remodeling in heart failure. Cardiovasc Res 2005;65(1):83-92. DOI: 10.1016/j.cardiores.2004.09.024.
12. Engelhardt S, Hein L, Keller U, Klämbt K, Lohse MJ. Inhibition of Na(+)-H(+) exchange prevents hypertrophy, fibrosis, and heart failure in beta(1)-

adrenergic receptor transgenic mice. Circ Res 2002;90(7):814-9. DOI: 10.1161/01.res.0000014966.97486.c0.
13. Baartscheer A, Schumacher CA, Wüst RC, Fiolet JW, Stienen GJ, Coronel R, Zuurbier CJ. Empagliflozin decreases myocardial cytoplasmic Na(+) through inhibition of the cardiac Na(+)/H(+) exchanger in rats and rabbits. Diabetologia 2017;60(3):568-573. DOI: 10.1007/s00125-016-4134-x.
14. Uthman L, Baartscheer A, Bleijlevens B, et al. Class effects of SGLT2 inhibitors in mouse cardiomyocytes and hearts: inhibition of Na(+)/H(+) exchanger, lowering of cytosolic Na(+) and vasodilation. Diabetologia 2018;61(3):722-726. DOI: 10.1007/s00125-017-4509-7.
15. Trum M, Riechel J, Lebek S, et al. Empagliflozin inhibits Na(+) /H(+) exchanger activity in human atrial cardiomyocytes. ESC Heart Fail 2020;7(6):4429-4437. DOI: 10.1002/ehf2.13024.
16. Weber S, Meyer-Roxlau S, Wagner M, Dobrev D, El-Armouche A. Counteracting Protein Kinase Activity in the Heart: The Multiple Roles of Protein Phosphatases. Front Pharmacol 2015;6:270. DOI: 10.3389/fphar.2015.00270.
17. Zhang H, Uthman L, Bakker D, et al. Empagliflozin Decreases Lactate Generation in an NHE-1 Dependent Fashion and Increases α-Ketoglutarate Synthesis From Palmitate in Type II Diabetic Mouse Hearts. Front Cardiovasc Med 2020;7:592233. DOI: 10.3389/fcvm.2020.592233.
18. Haetscher N, Feuermann Y, Wingert S, et al. STAT5-regulated microRNA-193b controls haematopoietic stem and progenitor cell expansion by modulating cytokine receptor signalling. Nat Commun 2015;6:8928. DOI: 10.1038/ncomms9928.
19. Chirumamilla CS, Fazil M, Perez-Novo C, et al. Profiling Activity of Cellular Kinases in Migrating T-Cells. Methods Mol Biol 2019;1930:99-113. DOI: 10.1007/978-1-4939-9036-8_13.
20. Yu G, Wang LG, Han Y, He QY. clusterProfiler: an R package for comparing biological themes among gene clusters. Omics 2012;16(5):284-7. DOI: 10.1089/omi.2011.0118.
21. Edgar AJ, Trost M, Watts C, Zaru R. A combination of SILAC and nucleotide acyl phosphate labelling reveals unexpected targets of the Rsk inhibitor BI-D1870. Biosci Rep 2014;34(1) DOI: 10.1042/bsr20130094.
22. Regier N, Frey B. Experimental comparison of relative RT-qPCR quantification approaches for gene expression studies in poplar. BMC Mol Biol 2010;11:57. DOI: 10.1186/1471-2199-11-57.
23. Gallagher S, Chakavarti D. Immunoblot analysis. J Vis Exp 2008(16):759. DOI: 10.3791/759.
24. Uthman L, Li X, Baartscheer A, et al. Empagliflozin reduces oxidative stress through inhibition of the novel inflammation/NHE/[Na(+)](c)/ROS-pathway in human endothelial cells. Biomed Pharmacother 2022;146:112515. DOI: 10.1016/j.biopha.2021.112515.

25. Hahn NE, Musters RJ, Fritz JM, et al. Early NADPH oxidase-2 activation is crucial in phenylephrine-induced hypertrophy of H9c2 cells. Cell Signal 2014;26(9):1818-24. DOI: 10.1016/j.cellsig.2014.04.018.
26. Abdulrahman N, Ibrahim M, Joseph JM, et al. Empagliflozin inhibits angiotensin II-induced hypertrophy in H9c2 cardiomyoblasts through inhibition of NHE1 expression. Mol Cell Biochem 2022;477(6):1865-1872. DOI: 10.1007/s11010-022-04411-6.
27. Li G, Zhao C, Fang S. SGLT2 promotes cardiac fibrosis following myocardial infarction and is regulated by miR-141. Exp Ther Med 2021;22(1):715. DOI: 10.3892/etm.2021.10147.
28. Lee SY, Lee TW, Park GT, et al. Sodium/glucose Co-Transporter 2 Inhibitor, Empagliflozin, Alleviated Transient Expression of SGLT2 after Myocardial Infarction. Korean Circ J 2021;51(3):251-262. DOI: 10.4070/kcj.2020.0303.
29. Ferté L, Marino A, Battault S, et al. New insight in understanding the contribution of SGLT1 in cardiac glucose uptake: evidence for a truncated form in mice and humans. Am J Physiol Heart Circ Physiol 2021;320(2):H838-h853. DOI: 10.1152/ajpheart.00736.2019.
30. Bischoff JR, Anderson L, Zhu Y, et al. A homologue of Drosophila aurora kinase is oncogenic and amplified in human colorectal cancers. Embo j 1998;17(11):3052-65. DOI: 10.1093/emboj/17.11.3052.
31. Smiles WJ, Catalano L, Stefan VE, Weber DD, Kofler B. Metabolic protein kinase signalling in neuroblastoma. Mol Metab 2023;75:101771. DOI: 10.1016/j.molmet.2023.101771.
32. Dutka M, Bobiński R, Francuz T, et al. SGLT-2 Inhibitors in Cancer Treatment-Mechanisms of Action and Emerging New Perspectives. Cancers (Basel) 2022;14(23):5811. DOI: 10.3390/cancers14235811.
33. Perry RJ, Shulman GI. Sodium-glucose cotransporter-2 inhibitors: Understanding the mechanisms for therapeutic promise and persisting risks. J Biol Chem 2020;295(42):14379-14390. DOI: 10.1074/jbc.REV120.008387.
34. Martinez EC, Passariello CL, Li J, Matheson CJ, Dodge-Kafka K, Reigan P, Kapiloff MS. RSK3: A regulator of pathological cardiac remodeling. IUBMB Life 2015;67(5):331-7. DOI: 10.1002/iub.1383.
35. Maekawa N, Abe J, Shishido T, et al. Inhibiting p90 ribosomal S6 kinase prevents (Na+)-H+ exchanger-mediated cardiac ischemia-reperfusion injury. Circulation 2006;113(21):2516-23. DOI: 10.1161/circulationaha.105.563486.
36. Yu W, Chen C, Cheng J. The role and molecular mechanism of FoxO1 in mediating cardiac hypertrophy. ESC Heart Fail 2020;7(6):3497-3504. DOI: 10.1002/ehf2.13065.
37. Sun X, Cao Z, Ma Y, Shao Y, Zhang J, Yuan G, Guo X. Resveratrol attenuates dapagliflozin-induced renal gluconeogenesis via activating the PI3K/Akt pathway and suppressing the FoxO1 pathway in type 2 diabetes. Food Funct 2021;12(3):1207-1218. DOI: 10.1039/d0fo02387f.
38. Darmellah A, Baetz D, Prunier F, Tamareille S, Rücker-Martin C, Feuvray D. Enhanced activity of the myocardial Na+/H+ exchanger contributes to left ventricular hypertrophy in the Goto-Kakizaki rat model of type 2 diabetes:

critical role of Akt. Diabetologia 2007;50(6):1335-44. DOI: 10.1007/s00125-007-0628-x.
39. Chen S, Khan ZA, Karmazyn M, Chakrabarti S. Role of endothelin-1, sodium hydrogen exchanger-1 and mitogen activated protein kinase (MAPK) activation in glucose-induced cardiomyocyte hypertrophy. Diabetes Metab Res Rev 2007;23(5):356-67. DOI: 10.1002/dmrr.689.
40. Lin K, Yang N, Luo W, et al. Direct cardio-protection of Dapagliflozin against obesity-related cardiomyopathy via NHE1/MAPK signaling. Acta Pharmacol Sin 2022;43(10):2624-2635. DOI: 10.1038/s41401-022-00885-8.
41. Kim I, Cho HJ, Lim S, Seok SH, Lee HY. Comparison of the effects of empagliflozin and sotagliflozin on a zebrafish model of diabetic heart failure with reduced ejection fraction. Exp Mol Med 2023;55(6):1174-1181. DOI: 10.1038/s12276-023-01002-3.
42. Guo H, Yu X, Liu Y, et al. SGLT2 inhibitor ameliorates endothelial dysfunction associated with the common ALDH2 alcohol flushing variant. Sci Transl Med 2023;15(680):eabp9952. DOI: 10.1126/scitranslmed.abp9952.
43. Jiang K, Xu Y, Wang D, et al. Cardioprotective mechanism of SGLT2 inhibitor against myocardial infarction is through reduction of autosis. Protein Cell 2022;13(5):336-359. DOI: 10.1007/s13238-020-00809-4.
44. Chung CC, Lin YK, Chen YC, Kao YH, Yeh YH, Trang NN, Chen YJ. Empagliflozin suppressed cardiac fibrogenesis through sodium-hydrogen exchanger inhibition and modulation of the calcium homeostasis. Cardiovasc Diabetol 2023;22(1):27. DOI: 10.1186/s12933-023-01756-0.
45. Chung YJ, Park KC, Tokar S, et al. Off-target effects of sodium-glucose co-transporter 2 blockers: empagliflozin does not inhibit Na+/H+ exchanger-1 or lower [Na+]i in the heart. Cardiovasc Res 2021;117(14):2794-2806. DOI: 10.1093/cvr/cvaa323.
46. Baker HE, Tune JD, Mather KJ, et al. Acute SGLT-2i treatment improves cardiac efficiency during myocardial ischemia independent of Na(+)/H(+) exchanger-1. Int J Cardiol 2022;363:138-148. DOI: 10.1016/j.ijcard.2022.06.054.
47. Zuurbier CJ, Baartscheer A, Schumacher CA, Fiolet JWT, Coronel R. Sodium-glucose co-transporter 2 inhibitor empagliflozin inhibits the cardiac Na+/H+ exchanger 1: persistent inhibition under various experimental conditions. Cardiovasc Res 2021;117(14):2699-2701. DOI: 10.1093/cvr/cvab129.
48. Chen S SC, van Amersfoorth S, Jan WT Fiolet, Baartscheer A, Veldkamp MW, Coronel R, Zuurbier CJ. Protease XIV abolishes NHE inhibition by empagliflozin in cardiac cells. Frontiers in Physiology 2023;14. DOI: 10.3389/fphys.2023.1179131.
49. Shi X, O'Neill MM, MacDonnell S, Brookes PS, Yan C, Berk BC. The RSK Inhibitor BIX02565 Limits Cardiac Ischemia/Reperfusion Injury. J Cardiovasc Pharmacol Ther 2016;21(2):177-86. DOI: 10.1177/1074248415591700.
50. Cuello F, Snabaitis AK, Cohen MS, Taunton J, Avkiran M. Evidence for direct regulation of myocardial Na+/H+ exchanger isoform 1 phosphorylation and

activity by 90-kDa ribosomal S6 kinase (RSK): effects of the novel and specific RSK inhibitor fmk on responses to alpha1-adrenergic stimulation. Mol Pharmacol 2007;71(3):799-806. DOI: 10.1124/mol.106.029900.

51. Jaballah M, Mohamed IA, Alemrayat B, Al-Sulaiti F, Mlih M, Mraiche F. Na+/H+ exchanger isoform 1 induced cardiomyocyte hypertrophy involves activation of p90 ribosomal s6 kinase. PLoS One 2015;10(4):e0122230. DOI: 10.1371/journal.pone.0122230.
52. Abdulrahman N, Jaspard-Vinassa B, Fliegel L, Jabeen A, Riaz S, Gadeau AP, Mraiche F. Na(+)/H(+) exchanger isoform 1-induced osteopontin expression facilitates cardiac hypertrophy through p90 ribosomal S6 kinase. Physiol Genomics 2018;50(5):332-342. DOI: 10.1152/physiolgenomics.00133.2017.
53. Catozzi S, Di-Bella JP, Ventura AC, Sepulchre JA. Signaling cascades transmit information downstream and upstream but unlikely simultaneously. BMC Syst Biol 2016;10(1):84. DOI: 10.1186/s12918-016-0303-2.
54. Choi J, Matoba N, Setoyama D, et al. The SGLT2 inhibitor empagliflozin improves cardiac energy status via mitochondrial ATP production in diabetic mice. Commun Biol 2023;6(1):278. DOI: 10.1038/s42003-023-04663-y.
55. Peng X, Li L, Lin R, et al. Empagliflozin Ameliorates Ouabain-Induced Na(+) and Ca(2+) Dysregulations in Ventricular Myocytes in an Na(+)-Dependent Manner. Cardiovasc Drugs Ther 2023;37(3):461-469. DOI: 10.1007/s10557-021-07311-x.
56. Onodi Z, Visnovitz T, Kiss B, et al. Systematic transcriptomic and phenotypic characterization of human and murine cardiac myocyte cell lines and primary cardiomyocytes reveals serious limitations and low resemblances to adult cardiac phenotype. J Mol Cell Cardiol 2022;165:19-30. DOI: 10.1016/j.yjmcc.2021.12.007.
57. Kuznetsov AV, Javadov S, Sickinger S, Frotschnig S, Grimm M. H9c2 and HL-1 cells demonstrate distinct features of energy metabolism, mitochondrial function and sensitivity to hypoxia-reoxygenation. Biochim Biophys Acta 2015;1853(2):276-84. DOI: 10.1016/j.bbamcr.2014.11.015.

Supplementary

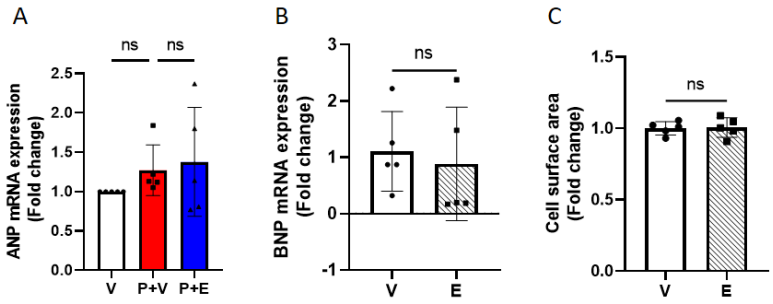

Supplementary Figure 1. PE-induced hypertrophy is not associated with increased ANP expression, and EMPA had no effect on BNP or cell surface area in healthy H9c2 cells.

A: Phenylepinephrine (P) without or with Empa (E) was without effect on cardiac ANP levels. One way ANOVA with Holm-Šídák's multiple comparisons test. **B-C**: Empa was without effect on BNP (**B**) or cell surface area (**C**) in untreated healthy H9c2 cells. Unpaired t test. Data are presented as mean ± SD. ns: not significant. (n=5 independent experiments).